ARMY RESEARCH LABORATORY

Modeling of the 35-mm Rarefaction Wave Gun

by Terence P. Coffee

ARL-TR-3792 **May 2006**

NOTICES

Disclaimers

The findings in this report are not to be construed as an official Department of the Army position unless so designated by other authorized documents.

Citation of manufacturer's or trade names does not constitute an official endorsement or approval of the use thereof.

Destroy this report when it is no longer needed. Do not return it to the originator.

Army Research Laboratory
Aberdeen Proving Ground, MD 21005-5066

ARL-TR-3792 **May 2006**

Modeling of the 35-mm Rarefaction Wave Gun

Terence P. Coffee
Weapons and Materials Research Directorate, ARL

REPORT DOCUMENTATION PAGE

Form Approved
OMB No. 0704-0188

1. REPORT DATE *(DD-MM-YYYY)*	2. REPORT TYPE	3. DATES COVERED (From - To)
May 2006	Final	May 2005–November 2005

4. TITLE AND SUBTITLE
Modeling of the 35-mm Rarefaction Wave Gun

5a. CONTRACT NUMBER

5b. GRANT NUMBER

5c. PROGRAM ELEMENT NUMBER

6. AUTHOR(S)
Terence P. Coffee

5d. PROJECT NUMBER
622624.H1A11

5e. TASK NUMBER

5f. WORK UNIT NUMBER

7. PERFORMING ORGANIZATION NAME(S) AND ADDRESS(ES)
U.S. Army Research Laboratory
ATTN: AMSRD-ARL-WM-BD
Aberdeen Proving Ground, MD 21005-5066

8. PERFORMING ORGANIZATION REPORT NUMBER
ARL-TR-3792

9. SPONSORING/MONITORING AGENCY NAME(S) AND ADDRESS(ES)

10. SPONSOR/MONITOR'S ACRONYM(S)

11. SPONSOR/MONITOR'S REPORT NUMBER(S)

12. DISTRIBUTION/AVAILABILITY STATEMENT
Approved for public release; distribution is unlimited.

13. SUPPLEMENTARY NOTES

14. ABSTRACT

The rarefaction wave gun (RAVEN) is designed to reduce the recoil momentum of a gun while having a minimal effect on the projectile velocity. The recoil reduction is achieved by venting gas out the breech through an expansion nozzle. This is similar to a recoilless rifle. The difference is that the venting is delayed until the projectile is some distance down tube. The opening of the breech creates a rarefaction wave that travels down the bore of the gun. If the timing is done correctly, the rarefaction wave will not reach the projectile until at or after muzzle exit. Hence, the projectile does not know the breech has opened, and the venting has no effect on the muzzle velocity.

As a proof of principal, a 35-mm RAVEN gun was designed, built, and fired. The breech is a moving piston. When the piston has moved a specified distance, it will open a vent into an expanding nozzle. There is a small reduction in the muzzle velocity due to the motion of the breech. That is, the chamber becomes larger than for a fixed breech gun. If the timing is correct, there is no additional reduction in the muzzle velocity due to the venting.

In this report, a one-dimensional model of the RAVEN is presented. The model covers the interior ballistics, the motion of the projectile and the breech, the opening of the vent, the flow through the nozzle, and the blow down of the gun. The model is validated against the 35-mm RAVEN data.

15. SUBJECT TERMS
rarefaction wave gun, interior ballistics, recoil

16. SECURITY CLASSIFICATION OF:			17. LIMITATION OF ABSTRACT	18. NUMBER OF PAGES	19a. NAME OF RESPONSIBLE PERSON
a. REPORT	b. ABSTRACT	c. THIS PAGE			Terence P. Coffee
UNCLASSIFIED	UNCLASSIFIED	UNCLASSIFIED	UL	46	19b. TELEPHONE NUMBER (*Include area code*) 410-278-6169

Contents

List of Figures iv

List of Tables vi

Acknowledgments vii

1. Introduction 1

2. The 35-mm Raven Fixture 1

3. The 35-mm Raven Code 3

3.1 Nonconformal Grid 4

3.2 Motion of the Projectile/Piston/Gun....5

3.3 Vent Opening 6

3.4 Boundary Conditions....7

3.5 Combustion 8

3.6 Time Step 8

4. The 35-mm Raven Data 9

5. Closed-Breech Cases 11

6. Nonventing Cases 14

7. Light-Piston Cases 17

8. Heavy-Piston Cases 21

9. Parametrics 25

10. Conclusions 29

11. References 30

Distribution List 31

List of Figures

Figure 1. RAVEN 35-mm assembly drawing. 2
Figure 2. RAVEN 35-mm internal working. 2
Figure 3. Numerical grid shortly after vent opening: nozzle (line), vector grid (dot), and piston (shaded). 7
Figure 4. Closed-breech shot 2-1-3: gauge P1 (line) and simulation (dot). 12
Figure 5. Closed-breech gun travel: shot 2-1-3 (line) and simulation (dot). 13
Figure 6. Closed-breech gun velocity: shot 2-1-3 (line) and simulation (dot) 14
Figure 7. Nonventing gun travel: shot 2-9-3 (line), shot 2-9-4 (dash), simulation 2-9-3 (dot), and simulation 2-9-4 (dot-dash). 15
Figure 8. Nonventing gun velocity: shot 2-9-3 (line), shot 2-9-4 (dash), simulation 2-9-3 (dot), and simulation 2-9-4 (dot-dash). 16
Figure 9. Shot 2-6-2; light piston, early vent, high-pressure group: gauge P1 (line) and simulation (dot). 18
Figure 10. Shot 2-6-3; light piston, early vent, low-pressure group: gauge P1 (line) and simulation (dot). 18
Figure 11. Gun travel; light piston, early vent, high-pressure group: shot 2-6-1 (line), shot 2-6-2 (dash), and simulation (dot). 19
Figure 12. Gun travel; light piston, early vent, low-pressure group: shot 2-6-3 (line) and simulation (dot). 19
Figure 13. Gun velocity; light piston, early vent, high-pressure group: shot 2-6-1 (line), shot 2-6-2 (dash), and simulation (dot). 20
Figure 14. Gun velocity; light piston, early vent, low-pressure group: shot 2-6-3 (line) and simulation (dot). 20
Figure 15. Shot 2-3-3; heavy piston, early vent, high-pressure group: gauge P1 (line) and simulation (dot). 22
Figure 16. Shot 2-3-4; heavy piston, early vent, low-pressure group: gauge P1 (line) and simulation (dot). 22
Figure 17. Gun travel; heavy piston, early vent, high-pressure group: shot 2-3-3 (line), shot 2-3-5 (dash), and simulation (dot). 23
Figure 18. Gun travel; heavy piston, early vent, low-pressure group: shot 2-3-4 (line) and simulation (dot). 23
Figure 19. Gun velocity; heavy piston, early vent, high-pressure group: shot 2-3-3 (line), shot 2-3-5 (dash), and simulation (dot). 24

Figure 20. Gun velocity; heavy piston, early vent, low-pressure group: shot 2-3-4 (line) and simulation (dot).....24

Figure 21. Gun velocity; light piston; gun resistance; closed breech (line), nonventing (dot), no gun resistance, closed breech (dash), and nonventing (dot-dash).....26

List of Tables

Table 1. Recoil distances to vent for different configurations. 3
Table 2. Recoil masses for different configurations. 3
Table 3. Experimental results: maximum chamber pressure (MPa), muzzle velocity (m/s), and free-recoil velocity (m/s). 10
Table 4. Bore resistance profile. 11
Table 5. Closed-breech gun; comparison of experimental and model results. 14
Table 6. Piston resistance profile. 15
Table 7. Nonventing gun; comparison of experimental and model results. 17
Table 8. Light piston; comparison of experimental and model results. 21
Table 9. Heavy piston; comparison of experimental and model results. 25
Table 10. Light piston; gun resistance; comparison of simulations 26
Table 11. Light piston; no gun resistance; comparison of simulations 27
Table 12. Heavy piston; no gun resistance; comparison of simulations. 27
Table 13. Small piston (scaled heavy piston); no gun resistance; comparison of simulations. 28
Table 14. Small piston (scaled heavy piston); no gun resistance; vary the distance from the vent opening to the nozzle exit. 29

Acknowledgments

The author would like to thank John McNeil for supplying RAVEN information and data and for his useful review of this manuscript.

INTENTIONALLY LEFT BLANK.

1. Introduction

Present large-caliber guns require a heavy mount to absorb the recoil. However, the emphasis in the U.S. Army is now on lightweight and deployable vehicles. The rarefaction wave gun (RAVEN) was invented by Kathe (*1*) as a means to substantially reduce the recoil, and hence the mass of the system that absorbs the recoil, while minimally reducing the projectile velocity. This is accomplished by venting the breech through an expansion nozzle during the firing cycle. If the timing is done correctly, the rarefaction wave from the venting will not reach the projectile until muzzle exit. Hence, the projectile does not know that the vent has opened.

This report discusses the modeling of the RAVEN concept. Guns are often modeled using a lumped parameter code, such as IBHVG2 (*2*). The interior ballistics is approximated by a series of ordinary differential equations. This requires an approximation to the velocity and pressure gradient in the gun, such as Lagrange or Pidduck-Kent. The gradient in a RAVEN is much more complicated. A lumped-parameter model was used by Kathe (*1*), but the model only worked up to muzzle exit. The model could not be used to calculate the recoil velocity.

Next in complexity is a one-dimensional (1-D) model. XKTC is a commonly used code (*3*). XKTC includes a number of phenomena that can not be modeled using a lumped-parameter code, such as flame spreading, grain fracture, and propellant drag. The code as written cannot handle a moving breech or venting through the breech.

Two- or three-dimensional problems can be done using NGEN (*4*). Again, the code as written does not include a moving breech or a nozzle. The run times are much longer then for a 1-D model.

A new 1-D model was developed that explicitly models the motion of the piston and the flow out of the vent. The free recoil velocity can be calculated. The model was validated against the 35-mm data.

2. The 35-mm Raven Fixture

Figure 1 shows an assembly drawing of the 35-mm RAVEN. The starting point is a 35-mm KD series anti-aircraft gun (*5*). The chamber diameter is 55 mm, so there is substantial chambrage. The propellant is a proprietary single perf deterred grain.

The moving breech/piston is in the shape of a delta wing. The breech is held into place by a shear plug (figure 2). The shear plug is designed to shear at a pressure of 220 MPa. The chamber plug determines how far the piston moves before opening the vent into the expansion nozzle. Table 1 gives the recoil distances to venting for the four configurations tested.

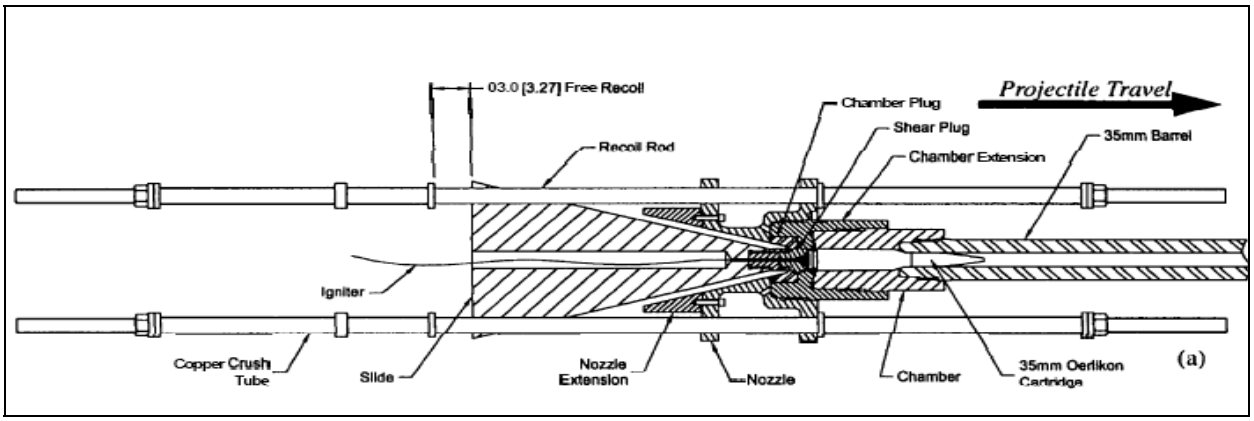

Figure 1. RAVEN 35-mm assembly drawing.

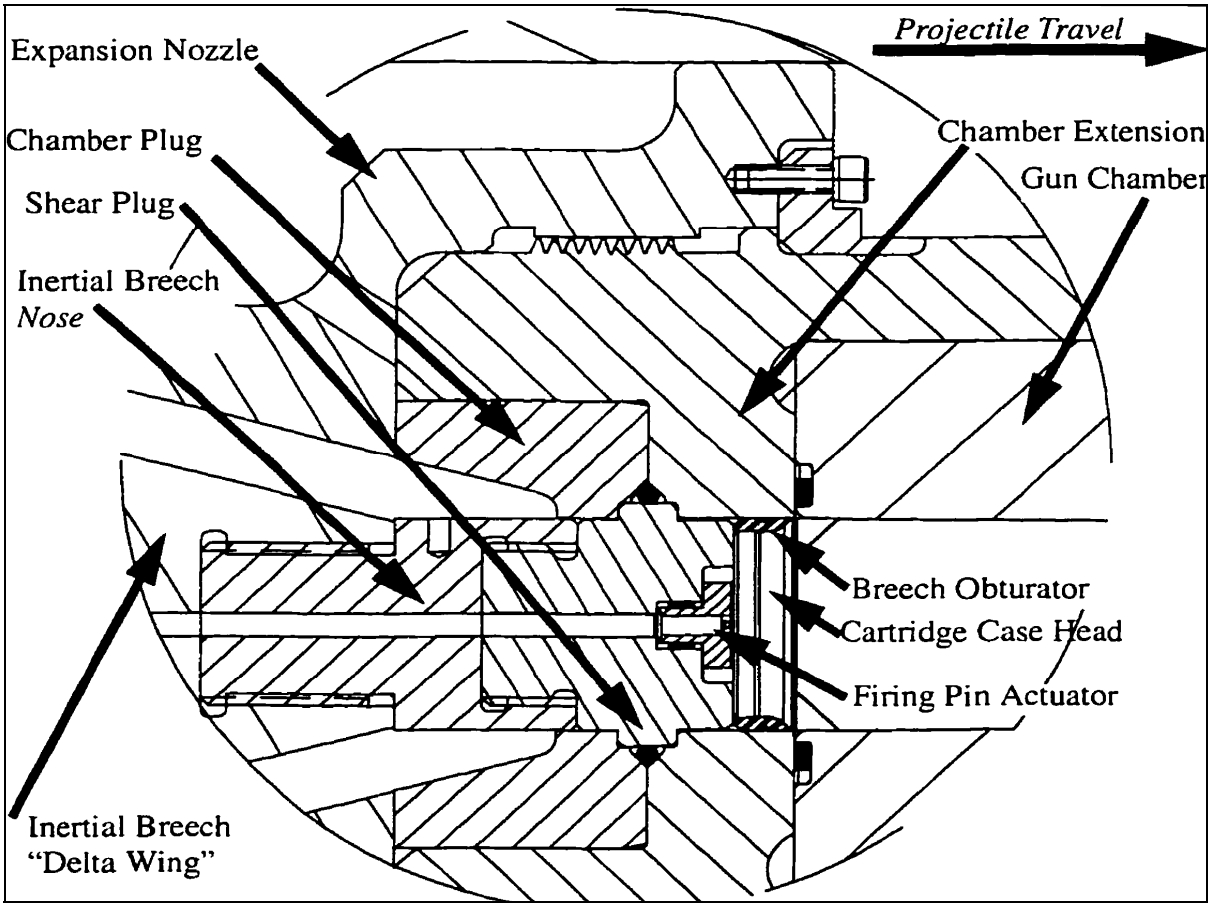

Figure 2. RAVEN 35-mm internal working.

Table 1. Recoil distances to vent for different configurations.

Name	Distance to Vent (mm)
Early	48.88
Nominal	56.37
Intermediate	75.31
Late	94.25

There were two different pistons (light and heavy) used in the tests with venting. There was also a piston used without a vent. A T-bar replaced the delta wing. Finally, the fixture was shot in a closed-breech configuration. The heavy piston was used, but with a steel shear plug instead of an aluminum plug, so the piston did not move. Table 2 gives the recoiling masses.

Table 2. Recoil masses for different configurations.

Configuration	Gun Mass (kg)	Piston Mass (kg)	Free-Recoil Mass (kg)
Closed breech	297.6	36.4	334.0
Light venting	297.6	20.9	318.5
Heavy venting	297.6	35.9	333.5
Nonventing	405.9	31.8	437.7

A piston can move freely for 83.0 mm. Then it impacts two copper crush tubes (figure 1). The tubes are designed to bring the piston to a halt with respect to the gun tube within 30 ms. The free-recoil velocity is the velocity of the of the tube/piston system after the velocities equilibrate. The system utilizes a free-recoil mount. The mount provides for 25.9 mm of travel forward and 25.4 mm of travel rearward. The free-recoil velocity is measured after the tube and the piston equilibrate and before the gun hits the ring-spring recoil arrestors.

3. The 35-mm Raven Code

A new 1-D code Rarefaction Wave Recoil (RAR) has been developed to model the interior ballistics and recoil of the RAVEN. The code is loosely based on previous work modeling liquid propellant guns (*6*, *7*).

The basic approach is a finite volume arbitrary Lagrangean-Eulerian (ALE) code. The computational domain is split into volumes. The scalar quantities (pressure, temperature, etc.) are assumed constant inside each volume, with a jump at the boundaries of the volume. The velocities are defined on the boundaries of the finite volumes (vector grid points). For a 1-D code, the velocities are only axial. Radial velocities in the chamber and nozzle are ignored.

To take a time step, the velocities are updated based on the pressure differences (momentum equation). The grid moves at these velocities (Lagrangean part of the time step). The scalar volumes are modified based on the new grid point positions. The scalar quantities are updated

based on the volume changes and the combustion. Then, the grid is moved to its final position. An advection routine moves the scalar and vector quantities. If the grid always is returned to its original position, the code is Eulerian. If the grid always moves with the fluid, the code is Lagrangean, and no advection is required.

In previous work, the grid has always been conformal (attached to the boundaries). For instance, consider the motion of the projectile. There was a uniform grid from the chamber to the base of the projectile. As the projectile moves, the grid stretches. When the grid becomes longer then a specified value, a new control volume is added using interpolation.

This procedure cannot be used for the RAR code. The major problem is the moving breech. As the vent opens, gas will flow between the piston and the nozzle. The piston and the nozzle move at different velocities. It is impossible to use a conformal grid. A secondary problem is the projectile. The next generation 105-mm RAVEN is expected to use a projectile with a long boat tail protruding into the chamber.

3.1 Nonconformal Grid

The RAR code requires a nonconformal grid. A 1-D grid (with area changes) is set up from the nozzle end to the muzzle end. The grid does not move (with respect to the gun). The projectile and piston will move through the grid. The scalar control volumes are numbered from i = 1 (nozzle end) to i = nx-1 (muzzle end). The vector grid points are numbered from i = 1 to i = nx. So, for instance, the pressure in the scalar control volume i (p_i) is between the velocities v_i and v_{i+1}.

The input now includes the shape and initial location of the piston and projectile. A new subroutine volsplit splits each scalar control volume into propellant volume (gas and unburnt propellant grains) and metal volume (piston or projectile). It also splits the areas at the vector grid points (finite volume boundaries) into propellant area and metal area.

The initiation subroutine initial is slightly more complicated than before. The propellant grains are spread evenly between the piston and the projectile, as well as the primer (assumed to be already gas). This routine uses the results from volsplit to compute how much propellant and gas goes into each scalar control volume, based on how much of the control volumes are taken up by metal. Before the piston and after the projectile, air is inserted at atmospheric pressure and temperature.

There is a fundamental numerical problem. The integration is explicit, so there is a Courant condition. The time step cannot be larger then the length of a control volume divided by the sound speed plus the gas velocity. That is, a sound wave cannot move more then one control volume in one time step.

Now consider a simple cylindrical projectile. The projectile is moving through a fixed grid. Consider what happens when the projectile just passes through a vector grid point and opens up

the next scalar control volume. The part of the new volume that is gas/propellant is very small. The effective length of this control volume is very small. This will require a very small time step until the projectile moves and opens up more of the control volume.

A new subroutine combine is used to get around the time-step limitation. This subroutine goes through the grid and looks for control volumes that are less then 10% propellant (more than 90% metal). Given certain boat tail shapes and grids, there may be more then one such control volume in succession. It then combines these control volumes with a preceding control volume (if to the left of piston/projectile) or a subsequent control volume. The scalar quantities in the control volumes are averaged. The velocities are found by interpolation.

3.2 Motion of the Projectile/Piston/Gun

There are three moving parts in the 35-mm RAVEN; the projectile, the piston, and the gun. Input to the code includes the projectile resistance pressure p_j as a function of projectile travel, the piston-resistance pressure p_s as a function of piston travel, and the gun-resistance pressure p_g as a function of gun travel. The projectile resistance is due to the force required to engrave the projectile rotating band and the friction down the tube. The piston resistance is first due to the shear plug and later due to the crush tubes. The gun resistance is due to friction between the gun and the mount. Note that for computing the projectile and piston resistance, the projectile and piston travels are taken to be relative to the position of the gun.

There are four cases. Before the chamber pressure reaches the projectile shot-start pressure or the piston-shear pressure, none of the masses move. Normally, the projectile will start to move before the piston. The projectile moves forward and the piston/gun recoils as a unit. Note that this occurs before the piston shears, and also after the crush tubes bring the piston to a halt with respect to the gun. It is possible for the piston to shear before shot-start pressure. In this case, the projectile and gun will move forward as a unit and the piston will move backward. This is not expected to occur in practice. Finally, all three masses can move independently.

Consider the general case where all three masses move independently. Let A_i be the area of the nozzle/chamber/tube at the i'th vector grid point. Let AM_i be the area of metal (piston or projectile) at this point, and AP_i be the area that is not blocked by metal. The force on the projectile will be

$$F_j = \sum p_i (AM_{i+1} - AM_i) - p_j A_{nx+1} \ , \qquad (1)$$

where the summation is taken from the left to the right of the projectile. This includes the force on a general boat tail, the force due to the air being compressed in front of the projectile, and the resistance pressure.

Let A_p be the area at the right end of the piston (breech area). Let p_a be atmospheric pressure, which is assumed to be 0.1 MPa. Then the force on the piston will be

$$F_s = \sum p_i (AM_{i+1} - AM_i) + p_a AM_1 - p_j A_p . \quad (2)$$

The summation is from the left to the right of the piston. The resistance pressure is applied to the breech area. The new term takes into account the atmospheric pressure on the left of the piston, if the piston extends past the end of the computational domain. This is not necessary for the projectile. At muzzle exit the pressure on the base of the projectile is much higher then atmospheric pressure. This is not true for the piston. Before projectile exit, as the chamber pressure drops, the nozzle becomes over-expanded. The pressure at the end of the nozzle is under atmospheric pressure. So the pressure at the left end of the piston may not be negligible.

The force on the gun is given by

$$F_g = \sum \max(p_i, p_a)(A_i - A_{i+1}) - p_a(A_1 - A_{nx}) - p_s A_p + p_j A_{nx} \pm p_g A_p. \quad (3)$$

The summation is over the entire computational domain. In the nozzle, the pressure is taken to be the maximum of the local pressure and atmospheric pressure. When the nozzle is badly over-expanded, the flow will separate. This cannot be modeled by a 1-D code. However, if the pressure in the nozzle is under atmospheric pressure, the formula assumes the flow has separated, and atmospheric air has entered the nozzle. This correction makes a noticeable difference in the free-recoil velocity. The second term is the pressure on the outside of the gun. This has a substantial effect on the recoil velocity. The third term is the effect of the piston resistance. If there is resistance, the piston will pull the gun backwards. The fourth term is the effect of projectile resistance. Finally, the last term is the effect of the friction between the gun and the mount. This force acts opposite of the motion of the gun.

The problem is solved in the lab framework. So when the gun moves, the grid moves with the gun. Since the basic implementation is an ALE code, this is easy to do.

3.3 Vent Opening

When the piston travels a specified distance, the vent rapidly opens into a 30° nozzle (see figure 2). This is approximated in the code as a jump condition in the radius. Figure 3 shows the grid for an early open case. The dotted lines indicate the vector grid points. The scalar control volumes are between the dotted lines. The vent opens at –4.888 cm, where the radius jumps from 2.75 to 3.1145 cm. The area at the jump is computed using the smaller diameter (dotted line). The volume of the scalar control volume to the right is computed using the smaller diameter. The volume of the scalar control volume to the left is computed using the larger diameter.

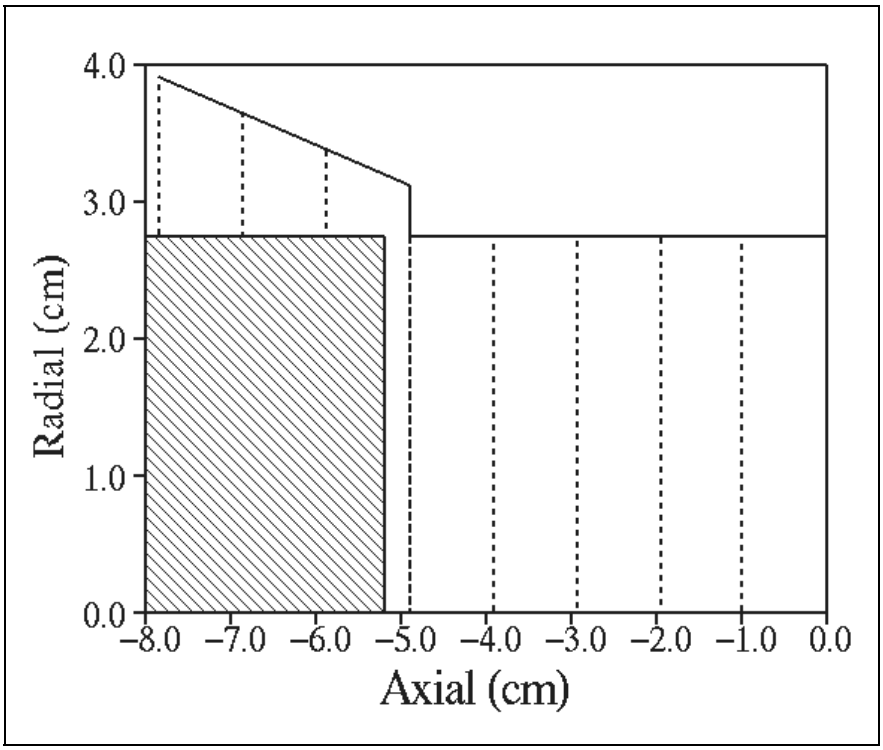

Figure 3. Numerical grid shortly after vent opening: nozzle (line), vector grid (dot), and piston (shaded).

There is an additional complication. In figure 3, the piston has just opened the vent. Consider the scalar control volume the right end of the piston is in. The area at the right is the chamber area. The area at the left is the area between the piston and the nozzle. But the physical minimum flow area is the space between the corner of the piston and the end of the chamber.

If this is ignored, the vent appears to open too quickly. As soon as the piston just clears the jump, the code thinks there is a large opening between the chamber and the nozzle. To fix this, the area between the right corner of the piston and the jump point is computed. The area at the left of the control volume is reduced to the minimum of the normal area and this new area. Material can flow into the control volume as soon as the piston passes the jump point, but it cannot pass quickly into the nozzle.

3.4 Boundary Conditions

Consider the flow out of the gun tube. When the projectile first exits, the flow will normally be supersonic. In this case, simple extrapolation is used, and the velocity at the boundary is set equal to the velocity one grid point before the boundary.

The flow quickly becomes subsonic. The flow out of the tube is assumed to be steady-state isentropic flow (*7*). If the outflow velocity is larger then the local sound speed, it must be lowered to the sonic velocity (choked flow). The flow will be choked for most of the blow-down phase.

Consider the flow out of the nozzle. Once into the expanding nozzle, the flow will be supersonic. If extrapolation is used to get the velocity at the nozzle exit, the gun will continue to empty until the pressure in the gun is well under atmospheric pressure. There is no way in a 1-D code to reverse the flow.

In reality, the flow will separate when the pressure becomes low enough. To roughly approximate this in the 1-D code, the pressure at the nozzle exit is tracked. If the flow is supersonic and the pressure in the first control volume is greater then atmospheric pressure, the velocity is extrapolated ($v_1 = v_2$). If the pressure in the first control volume is less then atmospheric pressure, the normal momentum equation is used. There will be flow into the nozzle. The material outside the nozzle is assumed to be air at atmospheric pressure and temperature. This is a crude approximation to separated flow, but should be adequate for computing recoil.

3.5 Combustion

The combustion model is copied from IBHVG2 (*2*). At time zero, the primer is assumed to be already combusted and the gas spread evenly through the gun. The burn rate of each grain is based on the mean pressure in the gun (average pressure between the right end of the piston and the left end of the projectile). The burn rate multiplied by the time step gives the depth of propellant burnt. A form function gives the surface area as a function of the amount of each grain burnt. The propellant is assumed to move with the gas (infinite drag).

The code has fewer capabilities than XKTC (*3*). However, if the charge is well behaved, this level of approximation is adequate.

A new form function is required for the single perf deterred grains in the 35-mm gun. Normally the deterrent is diffused into a grain, implying a gradual transition from the outer to the inner layer. In practice, however, the deterrent concentration is nearly constant in the deterred layer and falls off sharply at the boundary line (*8*). So the assumption is made that there is a sharp boundary between the outer and inner layers and the depth of the deterred layer is constant.

This led to the introduction of two new form functions. The outer layer form function behaves like a normal single perf grain, except a depth of the deterred layer is also entered. When that depth is reached, the outer layer is gone and the inner layer starts to combust. The initial dimensions of the inner layer are obtained from the dimensions of the initial grain and the depth of the deterred layer.

3.6 Time Step

Consider how the ideas previously listed fit together. To take a time step, first the control volumes are split into metal and gas/propellant. Also, the areas at the vector grid points are split into metal and gas/propellant. The heat loss to the gun tube is computed using a standard correlation (*7*). The velocity at the muzzle end of the gun is calculated. The gas/propellant

velocities are updated from the momentum equation. The velocity at the nozzle end is either computed from the momentum equation or from extrapolation. The velocities of the projectile, piston, and gun are updated. The volume of propellant burnt is calculated. The amount of gas and solid propellant is updated. The volumes of the scalar control volumes are temporarily modified based on the velocities and areas at each end (Lagrangean part of the time step). The scalar quantities are updated. The projectile, piston, and gun positions at the end of the time step are calculated. The grid is moved with the gun. The split of volumes and areas between metal and gas/propellant is recalculated for the new positions of the moving parts. Then material and momentum are advected through the boundaries as the Lagrangean grid is moved to the new position.

4. The 35-mm Raven Data

Table 3 summarizes the results for the experimental program. The first two columns give the configuration and the shot number. The third column gives the maximum pressure at the chamber gauge P1. This gauge is located 7.95 cm from the initial location of the breech. The gauges tended to drift negative over time, so the maximums are only approximate. The fourth column gives the muzzle velocity, recorded using ballistic screens.

The last column is the experimental free-recoil velocity. The data collected consisted of position measurements sampled every 0.01 ms. The data must be numerically differentiated to obtain the gun velocity. The velocity profile can be estimated by taking the difference of adjacent positions divided by the time step. However, negligible errors in the position become very large errors in the velocity. Kathe (*1*) used two filters to smooth the data. The coarse filter consisted of a 50-point running average that spanned half a ms. This filter is used to smooth the position data, the velocity is computed, and then the velocity is smoothed. The result still showed large numerical oscillations. The second filter consisted of a 300-point running average that spanned 3.0 ms. This was used to obtain the maximum gun velocity (free-recoil velocity). This smoothes the data, but will also limit the accuracy of the maximum.

In this report, a different procedure is used to smooth the data. The position profile is fitted by a parabolic spline. A spline is a piecewise polynomial. The polynomials are joined together at knot points. A parabolic spline is made up of second order polynomials. At the knot points, the curve is constrained to be continuous and smooth. The spline can then be differentiated analytically to obtain the velocity. After some experimentation, each polynomial is taken to be 3.0 ms long. If the pieces are shorter, there are numerical oscillations. The numbers obtained are similar but not identical to those computed by Kathe. The table gives the numbers computed using spline fits.

Table 3. Experimental results: maximum chamber pressure (MPa), muzzle velocity (m/s), and free-recoil velocity (m/s).

Configuration	Shot No.	Pressure (MPa)	Muzzle Velocity (m/s)	Recoil Velocity (m/s)
Closed breech	2-1-1	348	968	2.69
	2-1-2	334	1184	2.69
	2-1-3	346	1166	2.65
Nonventing	2-9-1	350	—	—
	2-9-2	—	1106	—
	2-9-3	337	—	2.35
	2-9-4	401	1135	2.43
Light early	2-6-1	408	1107	1.29
	2-6-2	404	1129	1.45
	2-6-3	328	1064	1.36
Light nominal	2-5-1	397	1131	1.42
	2-5-2	397	1130	1.53
	2-5-3	408	1116	1.51
Light inter	2-7-1	340	—	1.39
	2-7-2	343	1093	1.52
	2-7-3	331	1070	1.42
Light late	2-8-1	342	1085	1.68
	2-8-2	385	—	1.68
	2-8-3	328	1071	1.75
Heavy early	2-3-3	390	1164	1.77
	2-3-4	319	—	1.70
	2-3-5	402	1131	1.78
Heavy nominal	2-2-1	382	1128	1.76
	2-2-2	401	1165	1.75
	2-2-3	330	1128	1.70
	2-3-1	409	—	1.93
	2-3-2	409	—	1.88
Heavy inter	2-4-1	413	1143	2.05
	2-4-2	418	1155	1.98
	2-4-3	413	1194	2.02

The maximum chamber pressures fall into two groups. The high group has maximum pressures from 382 to 428 MPa. The low group has maximum pressures from 324 to 355 MPa. For the high group, the mean pressure is 402 MPa with a standard deviation of 9.86. For the low group, the mean pressure is 337 MPa with a standard deviation of 8.85. So the two groups are more than five standard deviations apart. The maximum pressure should change slightly, depending on whether there is a moving piston and how heavy the moving piston is. The location of the vent should have no effect on the maximum pressure, since all the vents open later than the pressure peak.

Next, consider just the light piston cases. The maximum pressures and muzzle velocities should be the same, independent of when the vent opens. Consider the cases where there is both a maximum pressure and a muzzle velocity. For the high group, the mean pressure is 403 MPa (standard deviation of 4.96), and the mean muzzle velocity is 1122.6 m/s (standard deviation of 9.52).

For the low group, the mean pressure is 334 MPa (standard deviation of 6.71), and the mean muzzle velocity is 1076.6 m/s (standard deviation of 10.71). The mean pressures are now 10 standard deviations apart. The mean velocities are four standard deviations apart. There is more scatter in the velocity measurements, but there is still a significant difference.

So there are clearly two different groups of experiments. This is possibly due to two different batches of propellant. Batches are not always repeatable. This is particularly true for deterred propellant. At this stage, it is impossible to know for certain what caused the differences.

5. Closed-Breech Cases

Consider first the closed-breech cases. The results should be the same as the baseline 35-mm gun results. The baseline gun has a muzzle velocity of 1175 m/s and a maximum chamber pressure of 383 MPa (*9*).

An estimate of the projectile shot start, engraving force, and bore friction is made in Kathe (*1*). Lacking any better information, this profile will be used for the projectile resistance (table 4).

Table 4. Bore resistance profile.

Projectile Travel (cm)	Resistance Pressure (MPa)
0.0	4.48
1.0	35.0
2.0	5.5
>2.0	5.5

The primer chemistry is unknown. The primer is assumed to be Benite. Following Kathe (*1*), it is assumed that the primer mass is 2.3 grain. As in IBHVG2, the primer is assumed to be completely burnt at time zero.

The charge is a proprietary single perf deterred grain. The chemical constituents are similar to M1 propellant (*1*). Nothing is known about the deterrent.

The deterrent layer is normally designed to burn out near peak pressure. Then, the faster burning inner layer starts to combust, keeping the pressure high. The longer the pressure can be kept near the peak, the more efficient the charge.

To begin with, the inner layer was assumed to have the same properties as M1, as reported in Kathe (*1*). The goal was to match the baseline gun's maximum chamber pressure and muzzle velocity, while having the outer layer burn out near maximum chamber pressure. After quite a bit of trial and error, the burn-rate exponent was increased from 0.71 to 0.78, the burn rate pre-exponential was increased slightly from 0.2175 to 0.224 cm/s, and the flame temperature was decreased from 2417 to 2200 K. The deterred layer is 0.13-mm thick. The burn rate of the

outer layer is 70% of the burn rate of the inner layer. Lacking other information, the chemistry of the outer layer is taken to be the same as the inner layer. The result is a maximum chamber pressure of 397 MPa and a muzzle velocity of 1167 m/s.

Figure 4 compares an experimental chamber pressure with the simulation. The experimental curve is moved over on the time axis to match the simulation at 200 MPa. The experiment has a maximum chamber pressure well under the value expected from the baseline gun. The recorded pressures are known to drift. At later times, the chamber pressure is lower than the pressures recorded by the gun-tube gauges, which cannot happen for a closed-breech gun. If the burn rate is modified to match the experimental pressure, the muzzle velocity becomes too low. The muzzle velocity can only be brought back up to the expected value by making the projectile resistance unreasonably small.

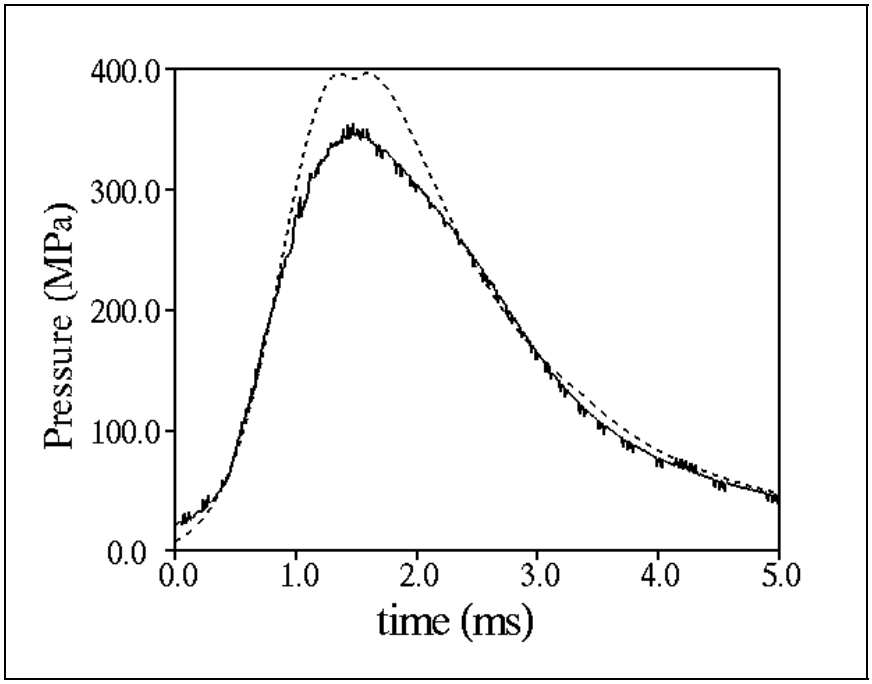

Figure 4. Closed-breech shot 2-1-3: gauge P1 (line) and simulation (dot).

So, in this report, no attempt will be made to match the maximum chamber pressure. The shape of the pressure profile, the time the vents open (when applicable), the muzzle velocity, and the free-recoil velocity are the values that will be matched, if possible.

Note that the simulation has a small double hump. The relative minimum between the pressure peaks indicates the point where the outer layer burns out. This is not seen in the experiment. This is probably an artifact of the model. In the simulation, all the propellant grains burn at the mean pressure. So the outer layer of all the grains will burn out at exactly the same time. In actuality, there will be a pressure gradient in the gun. So the burn out will not be as sharp in the experiment as in the simulation.

The calculated free-recoil velocity was initially 3.09 m/s, substantially high. This is possibly due to ignoring friction between the gun and the mount. The free-recoil velocity is reduced to 2.63 m/s if a constant gun resistance pressure of 4.0 MPa is included in the model. The resistance force is then 4.0× the breech area = $95.0\ MPa - cm^2$ = 9500 N-s.

Figure 5 compares the gun travel for the experiment and the simulation. The profiles are almost overlays at earlier times. Note that after 25.4 mm of travel, the gun will hit the ring-spring recoil arrestors. These are not in the simulation, so the profiles start to diverge.

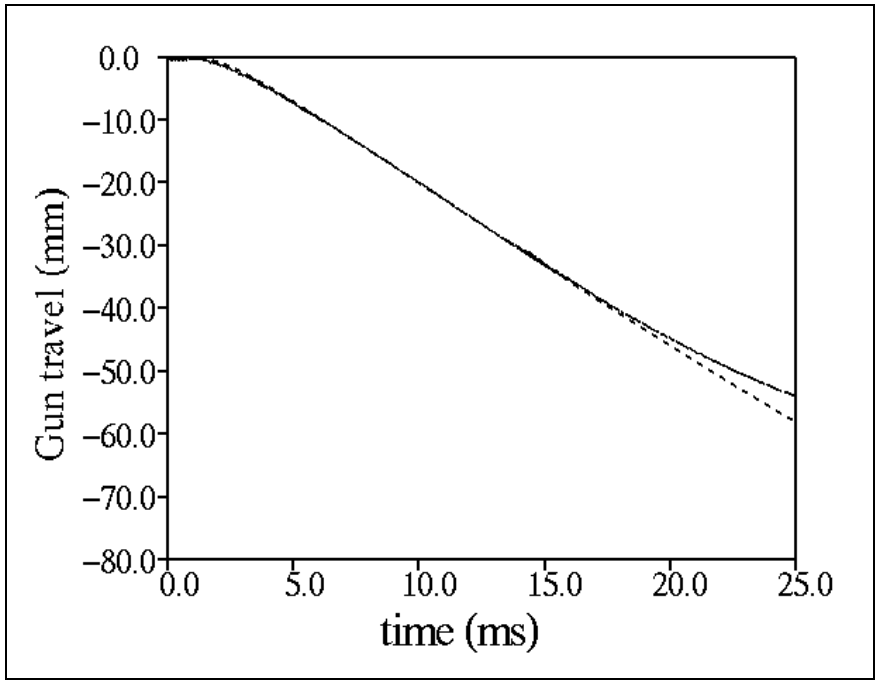

Figure 5. Closed-breech gun travel: shot 2-1-3 (line) and simulation (dot).

Figure 6 compares the gun velocity (free-recoil velocity) for the experiment and the simulation. Since the experimental gun travel has been fit by a parabolic spline, the gun velocity is piecewise linear. Given the limitations of the data, the agreement is good until the gun hits the recoil arrestors.

The other two closed-breech shots have virtually identical gun-travel profiles. The pressure profiles are slightly different. Table 5 summarizes the results. The simulation has a noticeably higher maximum chamber pressure then the experiment. The first experimental muzzle velocity is very low, and is not considered reliable. The muzzle velocity from the simulation is between the other two experimental muzzle velocities. The free recoil velocities are in good agreement. Of course, the model was designed to match the muzzle velocity and the free-recoil velocity. The test is whether the model will also match the other experiments.

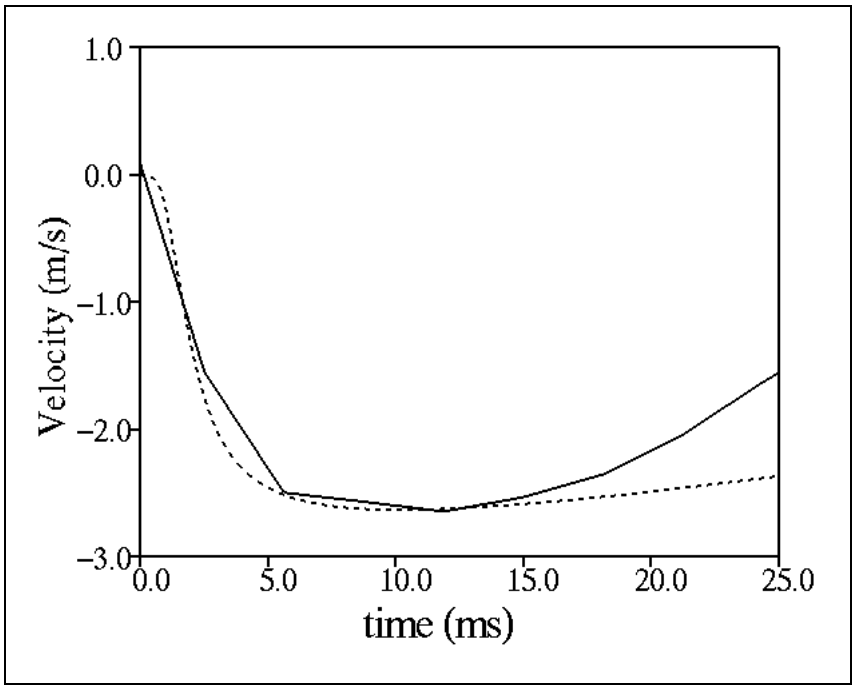

Figure 6. Closed-breech gun velocity: shot 2-1-3 (line) and simulation (dot).

Table 5. Closed-breech gun; comparison of experimental and model results.

Configuration	**Shot No.**	**Pressure (MPa)**		**Muzzle Velocity (m/s)**		**Recoil Velocity (m/s)**	
—	—	Experimental	Model	Experimental	Model	Experimental	Model
Closed breech	2-1-1	348	397	968	1167	2.69	2.63
—	2-1-2	334	397	1184	1167	2.69	2.63
—	2-1-3	346	397	1166	1167	2.65	2.63

6. Nonventing Cases

There were four shots with the nonventing moving breech. The gun does not have a nozzle. The piston is treated as a long cylinder. The gun motion was only recorded for the last two cases. Only these cases are considered here.

Shot 2-9-3 was in the low-pressure group, and shot 2-9-4 was in the high-pressure group. While the actual maximum pressures are suspect, the difference in the groups appears to be real (see section 4). All of the closed-breech shots were in the low-pressure group. To model the high-pressure group, the burn rate for the deterred layer is increased by 10%. This is based primarily on matching the venting cases.

The shear plug is designed to shear at 220 MPa. The shear web is 10 mm long. The resistance profile used is similar to the profile from Kathe (*1*). The resistance pressure drops rapidly when the shear plug fails, and then drops gradually to zero at 10 mm of travel (see table 6).

Table 6. Piston resistance profile.

Piston Travel (cm)	Resistance Pressure (MPa)
0.0	220
0.001	110
1.0	0
8.3	0
8.4	40
>8.4	40

At 8.3 cm of travel, the piston will hit the crush tubes. Each tube has a generally constant crush load of 55000 N-s (*1*). For both tubes, the resistance pressure would be 46.3 MPa. A value of 40 MPa is used instead, based on comparison with data.

Figure 7 shows the gun travels. The profiles are moved over in time to match at 5 mm of travel. Unlike the closed-breech cases, the gun first moves forward. When the shear plug gives way, the primary force on the gun is the chamber pressure acting on the chambrage. At 8.3 cm of piston travel (with respect to the gun), the piston hits the crush tubes. Then, momentum is transferred from the piston to the gun. When the piston and gun velocities equilibrate, the resulting velocity is the free-recoil velocity. This must be measured before the gun hits the recoil arrestors at 25.4 mm of travel.

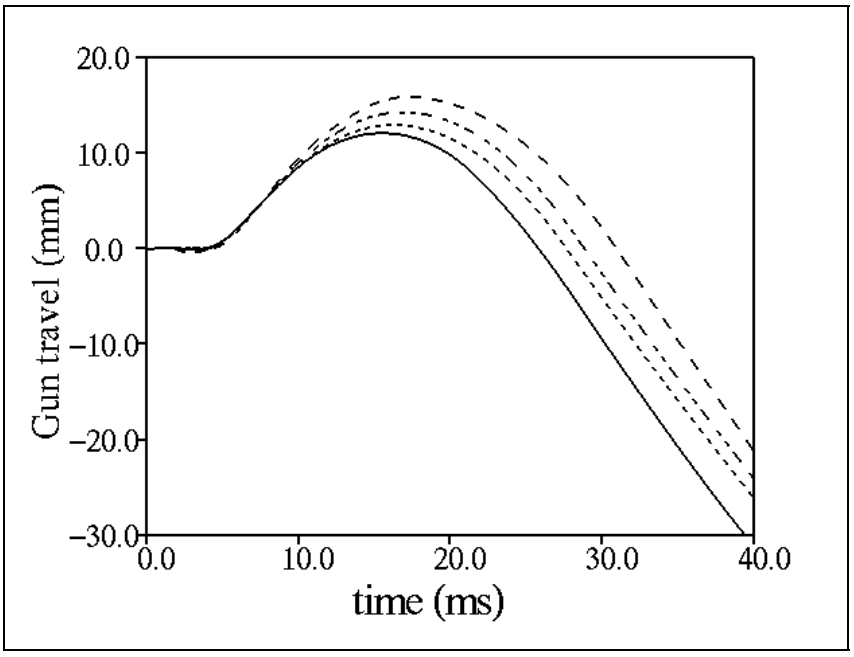

Figure 7. Nonventing gun travel: shot 2-9-3 (line), shot 2-9-4 (dash), simulation 2-9-3 (dot), and simulation 2-9-4 (dot-dash).

The two shots have different gun travels. The simulations indicate that the difference in chamber pressure will have much less of an effect. The indication is that the copper crush tubes are not repeatable.

Figure 8 shows the gun velocities. The minimum velocity is the free-recoil velocity. After reaching the minimum, both the experiments and the simulations indicate a decrease in the magnitude of the velocity. This is presumably due to friction between the gun and the mount. Shot 2-9-3 hits the recoil arrestors at ~37 ms, when the slope of the velocity shows a major change. Shot 2-9-4 does not hit the recoil arrestors until a later time.

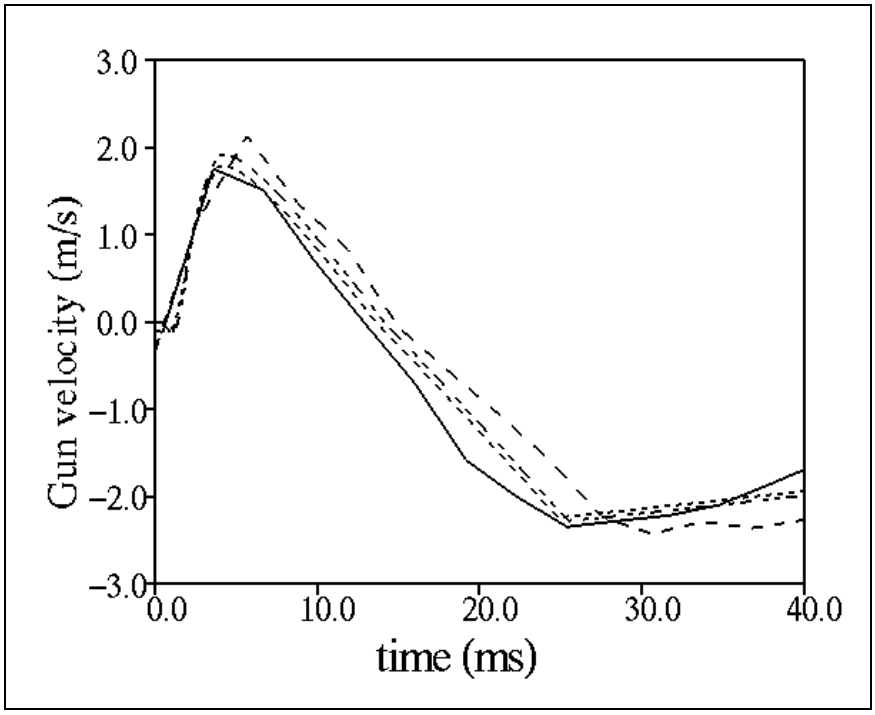

Figure 8. Nonventing gun velocity: shot 2-9-3 (line), shot 2-9-4 (dash), simulation 2-9-3 (dot), and simulation 2-9-4 (dot-dash).

Despite the difference in the gun travels, the difference in the experimental recoil velocities is small. As long as the crush tubes bring the piston to a halt (with respect to the gun) before the gun reaches the recoil arrestors, the momentum of the system will be about the same. The gun resistance will have a minor effect on the recoil velocity. That is, if the piston and gun velocities equilibrate slower, there will be more time for friction to slow down the gun before the gun reaches its maximum backward velocity.

The simulations can be made to match the experimental gun travels closely by adjusting the piston resistance pressure from the crush tubes. Since this has little effect on the recoil velocity, for simplicity a single piston resistance profile is used for all the moving piston cases (table 6).

The nonventing case is much less sensitive to the value used for gun friction then the closed-breech case. For instance, consider the simulation of shot 2-9-3. If the gun resistance is reduced from 4.0 to 0.0 MPa, the free-recoil velocity increases from 2.24 to only 2.27 m/s. For the closed-breech gun, the free-recoil velocity increases from 2.63 to 3.09 m/s. For the closed-breech gun, the friction always slows down the recoil. For the nonventing case, the gun first moves forward. Friction will slow down the initial forward motion as well as the later rearward motion. The frictional effects almost cancel out.

Table 7 summarizes the results. The agreement is reasonable, but not quite as good as for the closed-breech cases. Considering the uncertainty in the experimental recoil velocities, further refinement of the model is probably not helpful.

Table 7. Nonventing gun; comparison of experimental and model results.

Configuration	**Shot No.**	**Pressure (MPa)**		**Muzzle Velocity (m/s)**		**Recoil Velocity (m/s)**	
	—	Experimental	Model	Experimental	Model	Experimental	Model
Nonventing	2-9-3	337	388	—	1126	2.35	224
	2-9-4	401	449	1135	1159	2.43	228

7. Light-Piston Cases

For the vent-opening cases, the model includes a 30° expansion nozzle. The half angle (between the center line and the nozzle) is 15°. The diameter at the exit plane of the nozzle is ~23.65 cm.

The model requires the area of the piston as a function of distance from the breech end. The delta wing is a complicated shape, and it is not obvious how to obtain the area. So the piston is approximated by a long cylinder with a diameter of 5.5 chamber diameter (cm). Parametrics indicate that the exact area profile is not important, as long as there is a large area between the piston and the nozzle.

Figures 9 and 10 show the chamber pressures for two cases with a light piston and early vent opening. The maximum pressures, as expected, do not match. However, the simulations match very closely with the times that the vents open. The higher pressure case opens a little sooner then the lower pressure case.

Figures 11 and 12 show the gun travels. Again, the experimental travels are different for the three experiments. The simulations are qualitatively similar to the experiments.

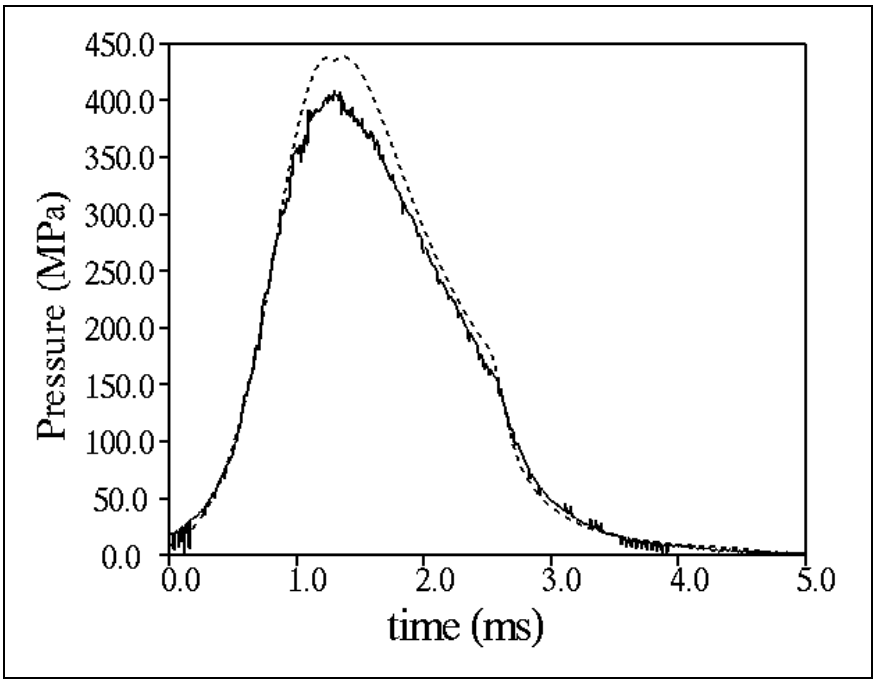

Figure 9. Shot 2-6-2; light piston, early vent, high-pressure group: gauge P1 (line) and simulation (dot).

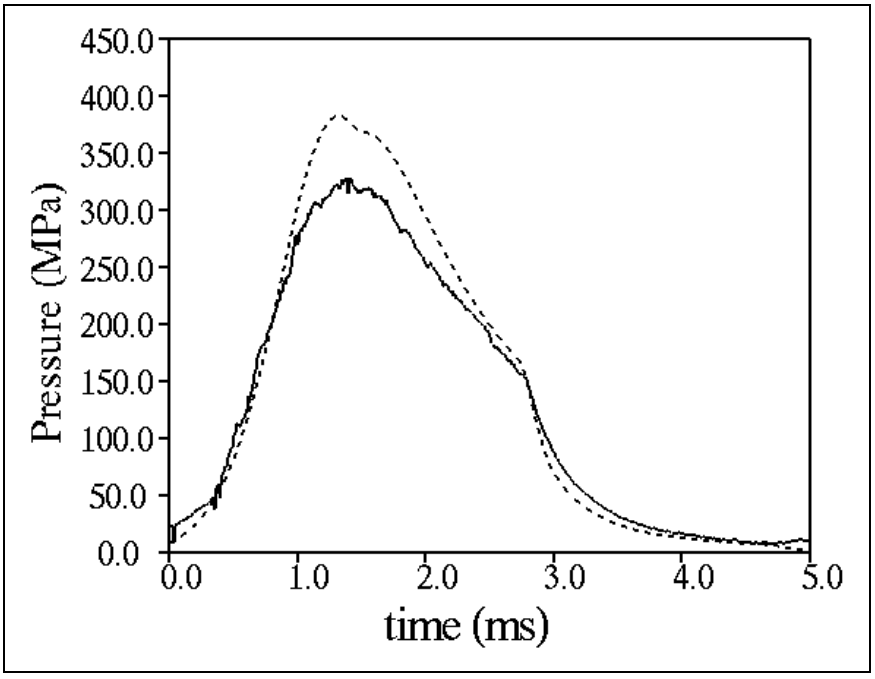

Figure 10. Shot 2-6-3; light piston, early vent, low-pressure group: gauge P1 (line) and simulation (dot).

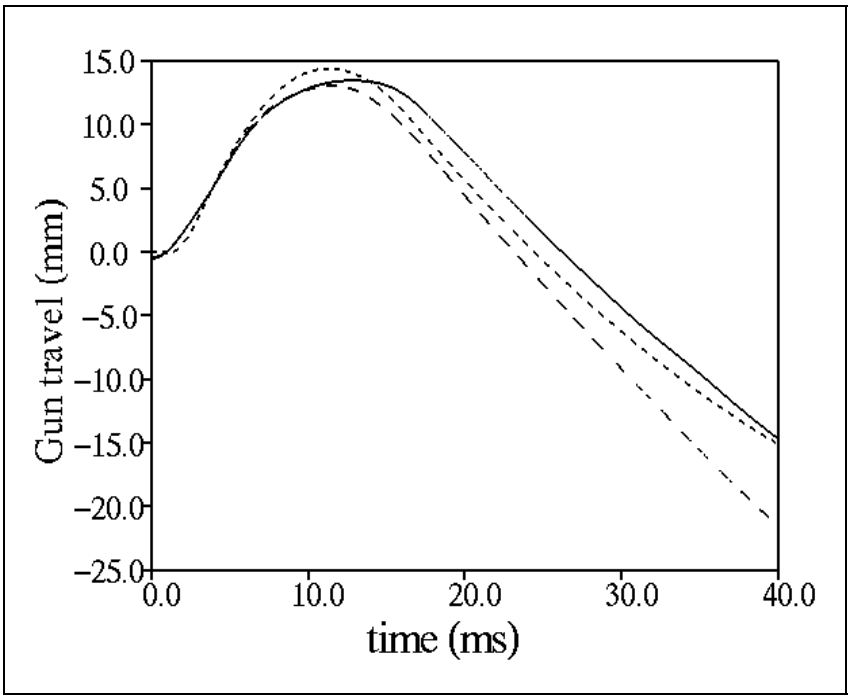

Figure 11. Gun travel; light piston, early vent, high-pressure group: shot 2-6-1 (line), shot 2-6-2 (dash), and simulation (dot).

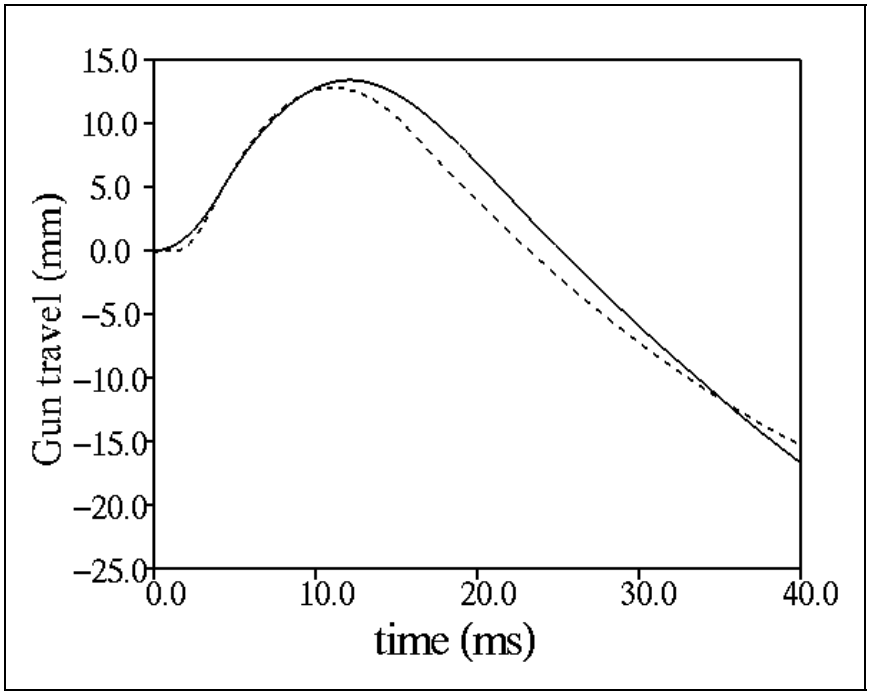

Figure 12. Gun travel; light piston, early vent, low-pressure group: shot 2-6-3 (line) and simulation (dot).

Figures 13 and 14 show the gun velocities. The minimum velocities are similar in magnitude. The slope of the velocity profiles at late times are larger for the simulations than for the experiments. This implies that the gun resistance pressure in the model is a little high at this stage.

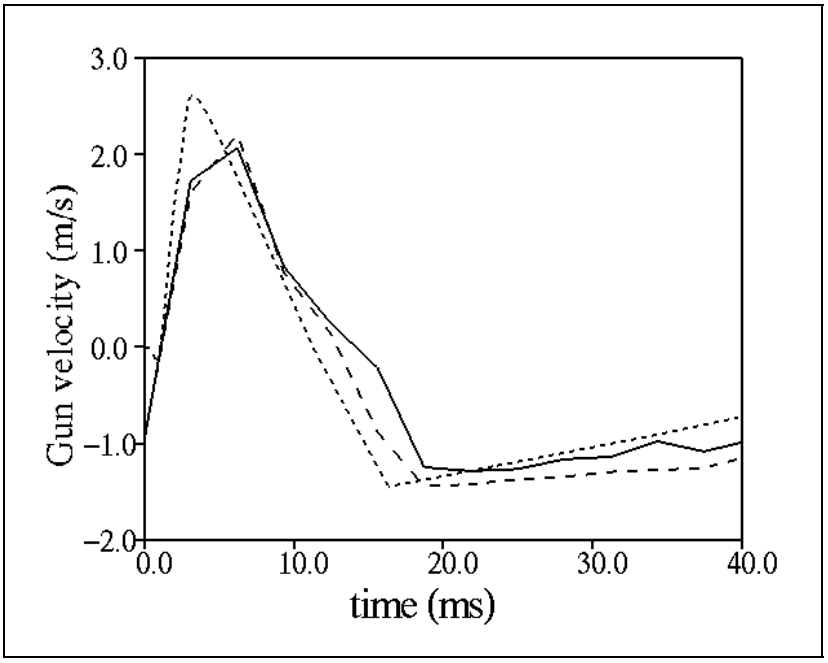

Figure 13. Gun velocity; light piston, early vent, high-pressure group: shot 2-6-1 (line), shot 2-6-2 (dash), and simulation (dot).

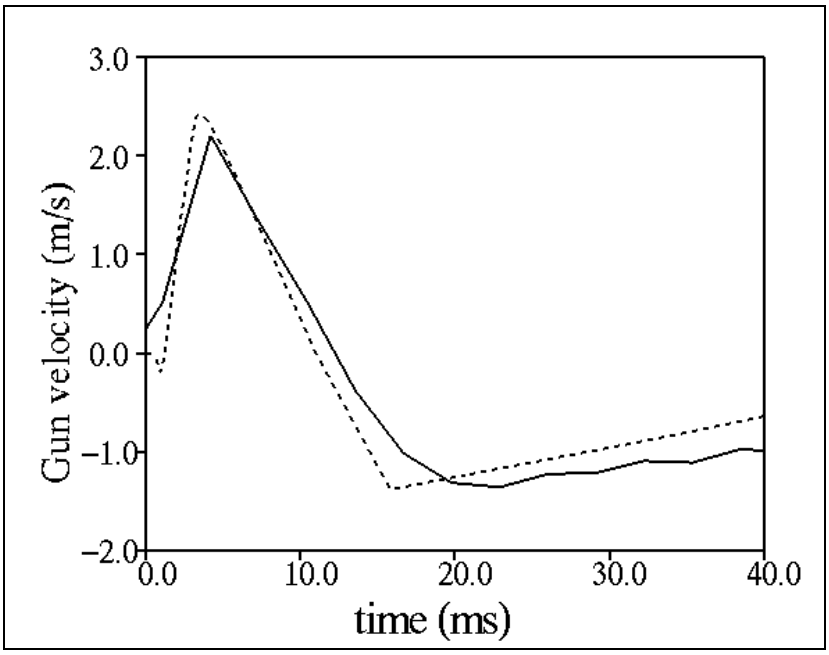

Figure 14. Gun velocity; light piston, early vent, low-pressure group: shot 2-6-3 (line) and simulation (dot).

The other light-piston cases show similar agreement between the experiments and the simulations. Table 8 summarizes the results. The free recoil velocities are in general a little higher in the simulations then in the experiments.

Table 8. Light piston; comparison of experimental and model results.

Configuration	**Shot No.**	**Pressure (MPa)**		**Muzzle Velocity (m/s)**		**Recoil Velocity (m/s)**	
	—	Experimental	Model	Experimental	Model	Experimental	Model
Light early	2-6-1	408	438	1107	1132	1.29	1.45
	2-6-2	404	438	1129	1132	1.45	1.45
	2-6-3	328	382	1064	1099	1.36	1.39
Light nominal	2-5-1	397	438	1131	1133	1.42	1.52
	2-5-2	397	438	1130	1133	1.53	1.52
	2-5-3	408	438	1116	1133	1.51	1.52
Light inter	2-7-1	340	382	—	1101	1.39	1.61
	2-7-2	343	382	1093	1101	1.52	1.61
	2-7-3	331	382	1070	1101	1.42	1.61
Light late	2-8-1	342	382	1085	1101	1.68	1.74
	2-8-2	385	438	—	1134	1.68	1.82
	2-8-3	328	382	1071	1101	1.75	1.74

8. Heavy-Piston Cases

The heavy piston does not move as rapidly at early times. This causes a slightly higher chamber pressure and muzzle velocity than the light piston cases. On the other hand, for a particular opening distance, the recoil reduction is less.

Figures 15 and 16 show the chamber pressures for two cases with a heavy piston and early vent opening. The maximum pressures, as expected, do not match. The simulations match very closely the times that the vents open.

Figures 17 and 18 show the gun travels. Again, the experimental travels are different for the three experiments. The simulations are qualitatively similar to the experiments.

Figures 19 and 20 show the gun velocities. The minimum velocities are similar in magnitude. The slope of the velocity profiles at late times are larger for the simulations then for the experiments.

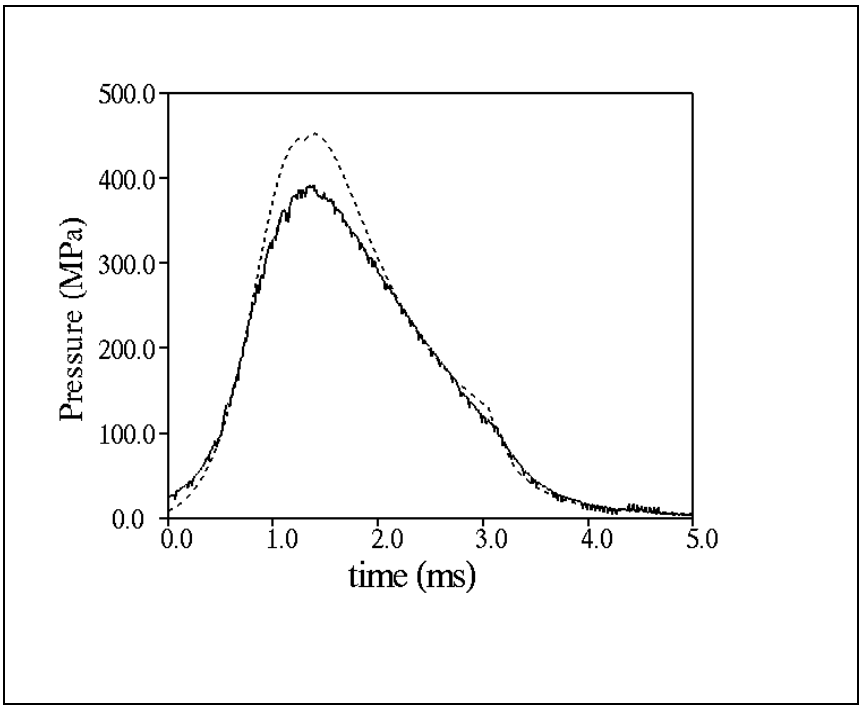

Figure 15. Shot 2-3-3; heavy piston, early vent, high-pressure group: gauge P1 (line) and simulation (dot).

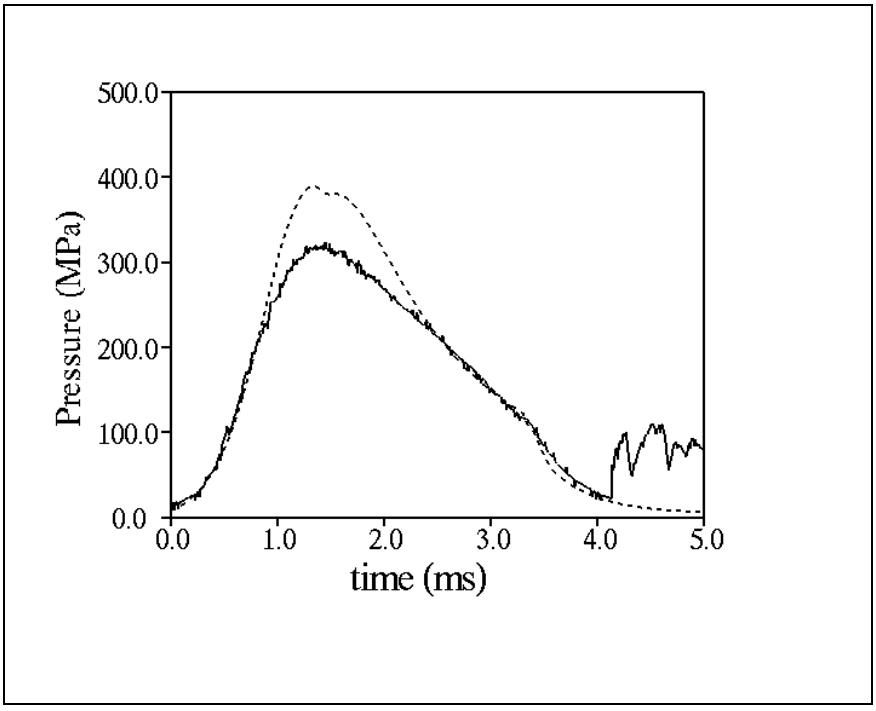

Figure 16. Shot 2-3-4; heavy piston, early vent, low-pressure group: gauge P1 (line) and simulation (dot).

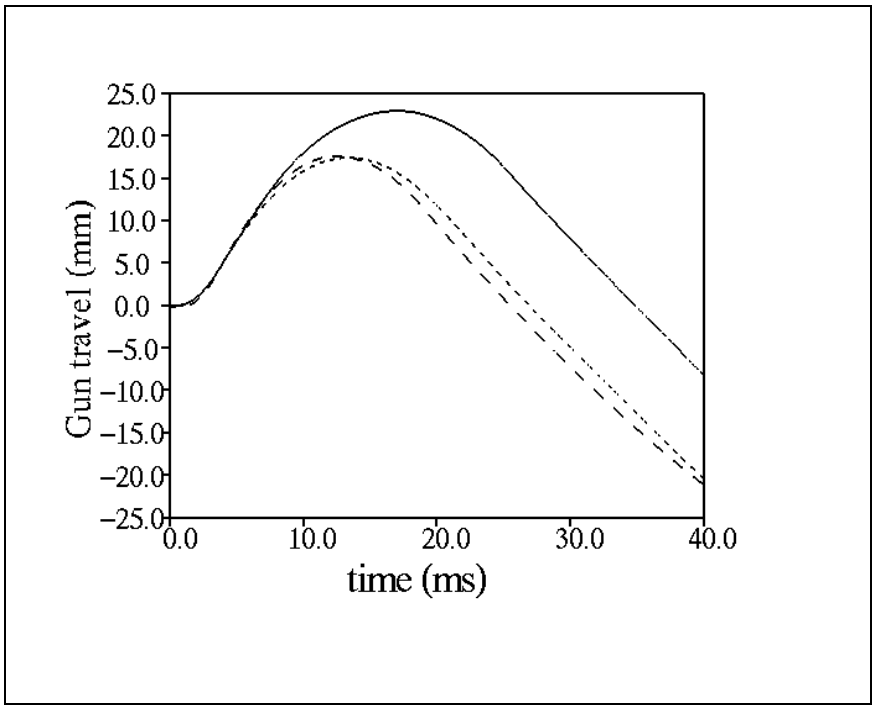

Figure 17. Gun travel; heavy piston, early vent, high-pressure group: shot 2-3-3 (line), shot 2-3-5 (dash), and simulation (dot).

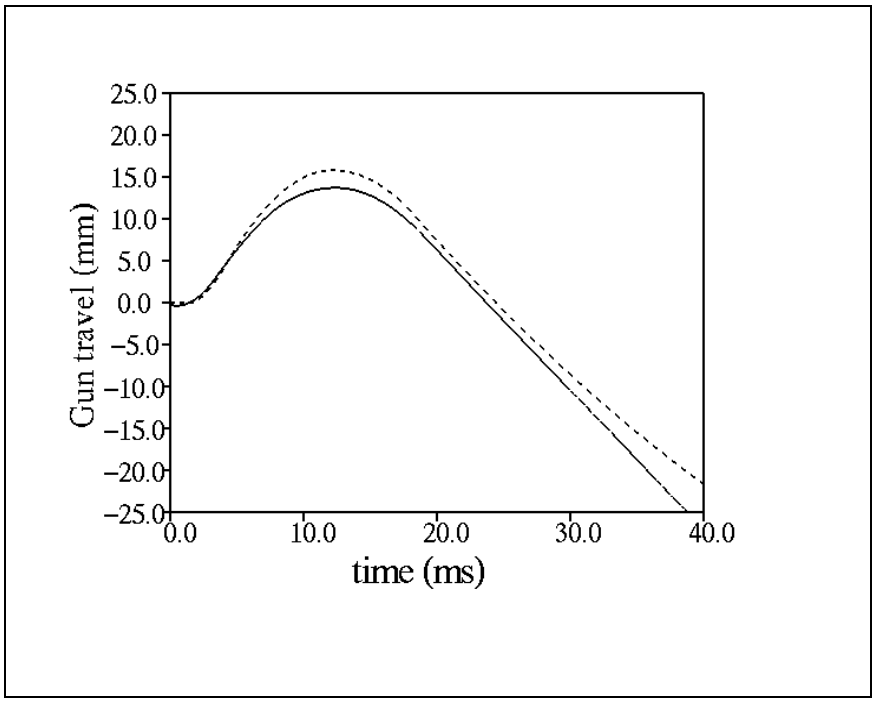

Figure 18. Gun travel; heavy piston, early vent, low-pressure group: shot 2-3-4 (line) and simulation (dot).

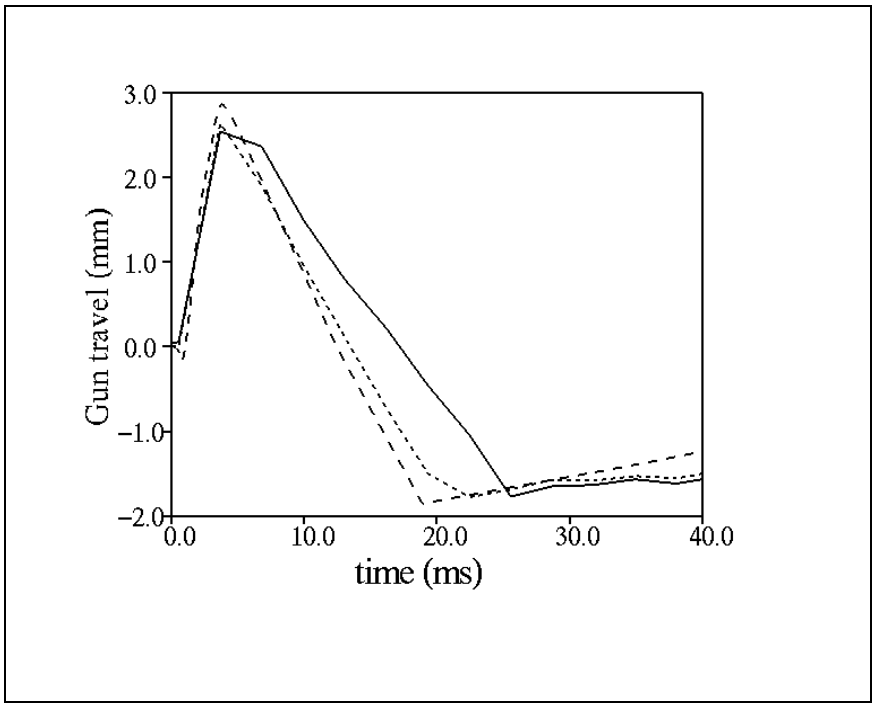

Figure 19. Gun velocity; heavy piston, early vent, high-pressure group: shot 2-3-3 (line), shot 2-3-5 (dash), and simulation (dot).

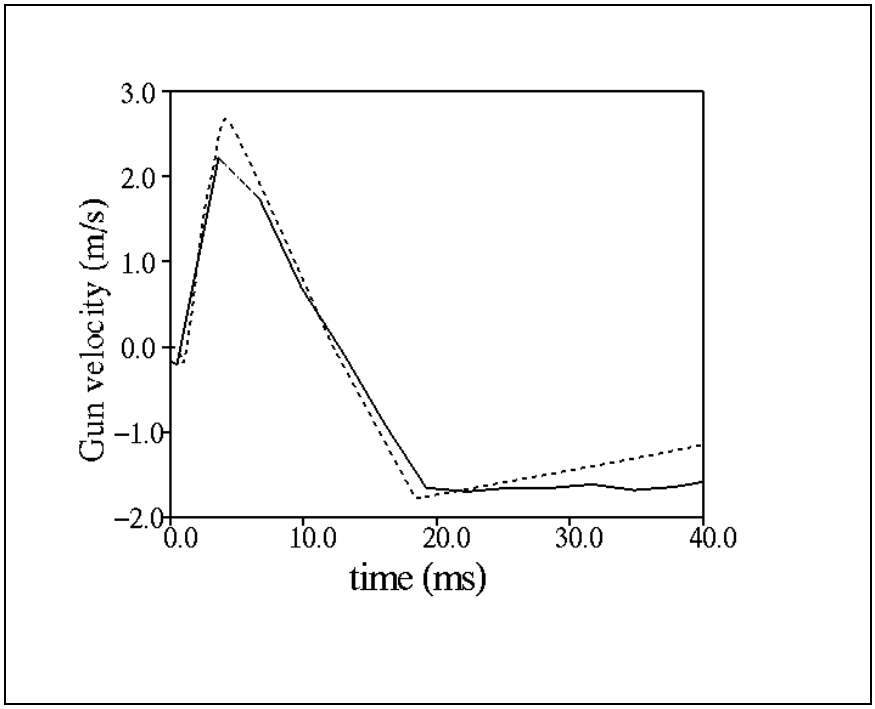

Figure 20. Gun velocity; heavy piston, early vent, low-pressure group: shot 2-3-4 (line) and simulation (dot).

The other heavy-piston cases show similar agreement between the experiments and the simulations. Table 9 summarizes the results. The free-recoil velocities are in general a little higher in the simulations then in the experiments.

Table 9. Heavy piston; comparison of experimental and model results.

Configuration	**Shot No.**	**Pressure (MPa)**		**Muzzle Velocity (m/s)**		**Recoil Velocity (m/s)**	
	—	Experimental	Model	Experimental	Model	Experimental	Model
Heavy early	2-3-3	390	452	1164	1163	1.77	1.85
	2-3-4	319	389	—	1130	1.70	1.78
	2-3-5	402	452	1131	1163	1.78	1.85
Heavy nominal	2-2-1	382	452	1128	1163	1.76	1.93
	2-2-2	401	452	1165	1163	1.75	1.93
	2-2-3	330	389	1128	1130	1.70	1.85
	2-3-1	409	452	—	—	1.93	1.93
	2-3-2	409	452	—	—	1.88	1.93
Heavy inter	2-4-1	413	452	1143	1163	2.05	2.08
	2-4-2	418	452	1155	1163	1.98	2.08
	2-4-3	413	452	1194	1163	2.02	2.08

9. Parametrics

In the experiments, the masses are different for the four cases (closed breech, nonventing, light piston, and heavy piston). Now that the code has been validated, it is possible to do more direct comparisons.

Consider first the light piston. The code is run with a closed breech and a nonventing piston, but with the gun mass (297.6 kg) and piston mass (20.9 kg) from the light piston cases. Then, the code is run for a venting piston with various opening times. The starting point is the early-open vent, where the vent opens at 4.888 cm of travel and the diameter jumps from 5.5 to 6.229 cm. The distance to the vent opening is varied. The diameter jump at the opening remains the same, as does the nozzle after the opening.

At first, the code was run with a constant gun resistance of 4.0 MPa, as with the previous calculations. Table 10 shows the results for the closed-breech case and the nonventing case. The table gives the maximum chamber pressure, the muzzle velocity, the free-recoil velocity, and the resulting momentum (units are kg-m/s = n-s). The results are unexpected. Even though the nonventing case has a lower maximum chamber pressure, the recoil velocity is higher.

Table 10. Light piston; gun resistance; comparison of simulations.

Configuration	Pressure (MPa)	Muzzle Velocity (m/s)	Recoil Velocity (m/s)	Momentum (N-s)
Closed breech	397	1167	2.76	880
Nonventing	383	1102	2.99	952

Figure 21 shows why this happens. The figure shows the gun velocities for the closed-breech and nonventing cases with and without gun resistance. The closed-breech gun recoils almost immediately. The frictional resistance than slows the gun down. The free-recoil velocity is much lower with frictional resistance than without frictional resistance. On the other hand, for the nonventing cases, most of the rearward momentum is initially in the piston. There is no friction between the piston and the mount. As momentum is transferred from the piston to the gun, the frictional resistance will start to have an effect. But the overall effect of the gun frictional resistance is small for the nonventing case.

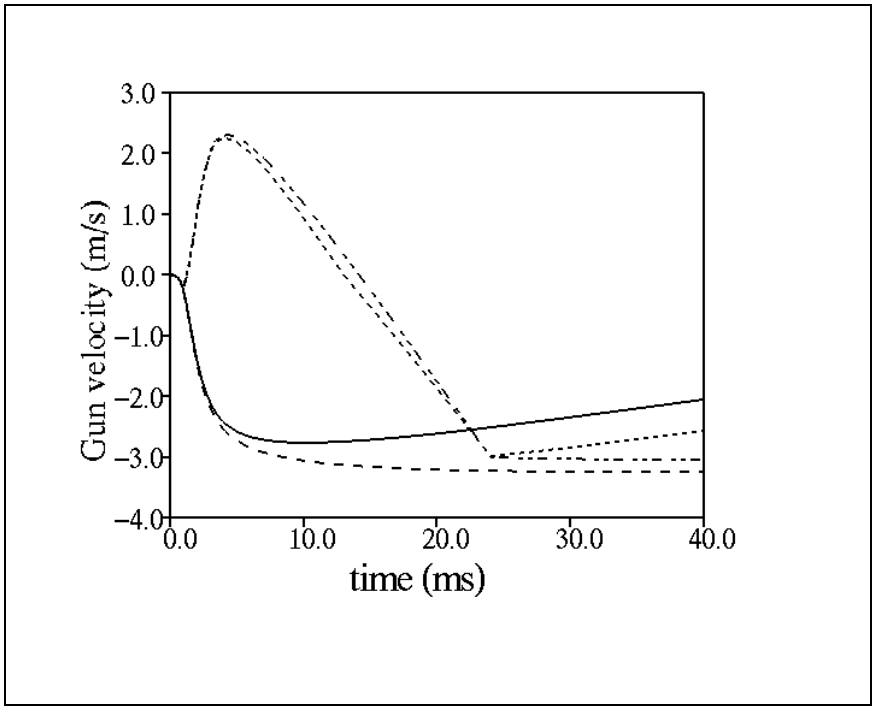

Figure 21. Gun velocity; light piston; gun resistance; closed breech (line), nonventing (dot), no gun resistance, closed breech (dash), and nonventing (dot-dash).

So, in order to examine the trends, calculations were made without gun resistance. Table 11 shows the results. Just by having a moving breech (nonventing piston), the pressure drops slightly and the muzzle velocity drops 5.5%. For the venting cases, the distance (cm) until the

vent opens is given. If the vent opens at 5.0 cm of piston travel, there is a negligible drop in muzzle velocity from the nonventing case and a 58% drop in recoil momentum. The recoil can be decreased even more if a lower muzzle velocity is acceptable.

Table 11. Light piston; no gun resistance; comparison of simulations.

Configuration	Pressure (MPa)	Muzzle Velocity (m/s)	Recoil Velocity (m/s)	Momentum (N-s)
Closed breech	397	1167	3.24	1033
Nonventing	383	1103	3.06	974
Vent 5.0	382	1099	1.29	410
Vent 4.0	382	1090	1.14	363
Vent 3.0	382	1064	0.96	305
Vent 2.0	382	1011	0.72	229

Similar calculations were then done using the heavy piston (table 12). For the closed breech, the recoil velocity is less because the recoiling mass is greater. The recoil momentum is the same for both pistons. For the nonventing case, the muzzle velocity only drops 3.1%. The heavier piston does not increase the chamber volume as rapidly. If the vent opens at 3.0 cm of piston travel, there is a negligible drop in muzzle velocity from the nonventing case and a 55% decrease in recoil momentum.

Table 12. Heavy piston; no gun resistance; comparison of simulations.

Configuration	Pressure (MPa)	Muzzle Velocity (m/s)	Recoil Velocity (m/s)	Momentum (N-s)
Closed breech	397	1167	3.10	1033
Nonventing	389	1131	2.99	999
Vent 5.0	389	1130	1.70	566
Vent 4.0	389	1130	1.55	517
Vent 3.0	389	1128	1.36	453
Vent 2.0	389	1110	1.10	366
Vent 1.8	389	1100	1.03	344
Vent 1.5	389	1080	0.92	307

It is possible to make a direct comparison by matching up the muzzle velocities. Consider the light piston with the vent opening after 5.0 cm of travel. The muzzle velocity is 1099 m/s and the recoil momentum is 410 n-s. Next, consider the heavy piston with the vent opening after 1.8 cm of travel. The muzzle velocity is 1100 m/s and the recoil momentum is 344 n-s. The recoil momentum can be reduced substantially by using the heavy piston. Of course, there may be other reasons why more mass is not desirable.

The drop in muzzle velocity is due to the motion of the piston, which increases the chamber volume. One way to minimize the muzzle velocity drop is to use a heavier piston. Another way is to use a piston with a smaller area.

A new configuration is investigated where the area of the piston is the same as the area of the gun tube. A reverse chambrage is put at the back of the chamber. The length of the chamber is increased slightly, so the initial chamber volume is unchanged. A moving piston is put at the smaller breech. This new small piston is a scaled heavy piston. The mass is reduced proportional to the area change. So the mass drops from 35.9 to 14.5 kg.

Table 13 shows the results. The closed-breech case has the same muzzle velocity as before (table 12). The recoil velocity is greater, since the total recoiling mass is less. The recoil momentum is almost the same. For the nonventing piston, the muzzle velocity drops only 1.2%.

Table 13. Small piston (scaled heavy piston); no gun resistance; comparison of simulations.

Configuration	Pressure (MPa)	Muzzle Velocity (m/s)	Recoil Velocity (m/s)	Momentum (N-s)
Closed breech	396	1167	3.30	1029
Nonventing	393	1153	3.25	1015
Vent 4.0	393	1152	2.01	626
Vent 3.0	393	1152	1.82	568
Vent 2.0	393	1140	1.55	485
Vent 1.9	392	1136	1.52	475
Vent 1.8	393	1132	1.49	465
Vent 1.7	392	1128	1.46	454

For the venting cases, the jump in diameter when the vent opens is kept proportional to the previous early open cases. That is, previously the diameter jumped from 5.5 to 6.229 cm. Now the diameter jumps from 3.5 to 4.0 cm. The length of the nozzle after the diameter jump is kept the same as before. Therefore the exit diameter of the nozzle is slightly less.

To allow for a direct comparison, consider a muzzle velocity of 1128 m/s. For the heavy piston (table 12) the corresponding recoil momentum is 453 n-s. For the small piston (table 13) the corresponding recoil momentum is 454 n-s, basically the same. But with the smaller piston, the system mass is less. With the smaller piston, it is also possible to have less of a reduction in muzzle velocity if less of a reduction in recoil momentum is acceptable.

The nozzle is under-expanded through most of the recoil process. The nozzle in the 35-mm gun might be longer than necessary. Parametrics were done to consider the effect of changing the length of the nozzle. The baseline is taken to be the smaller piston, with the vent opening at 1.7 cm of travel (last entry, table 13). The nozzle extends 32.5 cm past the vent opening. Table 14 shows the results for changing the nozzle length, while keeping a 15° half-angle nozzle. The table indicates that the nozzle length can be cut in half with only a 3% increase in the recoil momentum.

Table 14. Small piston (scaled heavy piston); no gun resistance; vary the distance from the vent opening to the nozzle exit.

Length (cm)	Exit Diameter (cm)	Muzzle Velocity (m/s)	Recoil Velocity (m/s)	Momentum (N-s)
15.0	12.038	1128	1.50	468
20.0	14.718	1128	1.48	462
25.0	17.397	1128	1.47	458
30.0	20.077	1128	1.46	455
32.5	21.417	1128	1.46	454
35.0	22.756	1128	1.45	454
40.0	25.436	1128	1.45	452

If the nozzle is modified, the mass of the system will also be modified. However, this has almost no effect on the recoil momentum, which depends on the force exerted on the gun and the piston, so it was not considered in the calculations. Reducing the length of the nozzle would presumably reduce the system mass.

10. Conclusions

A new 1-D code was written to model the RAVEN concept. The code includes explicitly the moving piston and flow out of the nozzle. The simulations were compared to a series of 35-mm RAVEN experiments. The propellant characteristic, piston resistance (shear plug and crush tubes), and gun resistance (friction) were not known. These were adjusted to match the data. The simulations were then in good agreement with the entire range of data (closed breech, nonventing, light piston, and heavy piston).

The RAVEN 35-mm fixture used a moving piston to open the flow out the breech. This necessarily reduced the muzzle velocity by increasing the chamber area. If timed correctly, the vent opening did not further reduce the muzzle velocity. The rarefaction wave from the breech does not reach the projectile until muzzle exit.

Parametric calculations indicate that a smaller breech is more efficient. In the experiments, the breech area was much larger then the gun-tube area (large chambrage). If the breech area is reduced to the gun-tube area, the recoil can be reduced by 50% with only a 2% reduction in the muzzle velocity. More recoil reduction is possible if the muzzle velocity can be further reduced.

The code will be used to help in the design of a proposed 105-mm RAVEN.

11. References

1. Kathe, E. L. Rarefaction Wave Gun Propulsion. Ph.D. Thesis, Rensselaer Polytechnic Institute, Troy, NY, 2002.

2. Anderson, R. D.; Fickie, K. D. *IBHVG2 - A User's Guide*; BRL-TR-2829; U.S. Army Ballistic Research Laboratory: Aberdeen Proving Ground, MD, July 1987.

3. Gough, P. S. *Interior Ballistics Modeling: Extensions to the One-Dimensional XKTC Code and Analytical Studies of Pressure Gradient for Lumped Parameter Codes*; ARL-CR-460; U.S. Army Research Laboratory: Aberdeen Proving Ground, MD, 2001.

4. Gough, P. S. *Initial Development of Core Module of Next Generation Interior Ballistic Model NGEN*; ARL-CR-234; U.S. Army Research Laboratory: Aberdeen Proving Ground, MD, 1995.

5. Chinn, G. M. *The Machine Gun, Volume V*; Edwards Brothers Publishing: Ann Arbor, MI, 1987.

6. Coffee, T. P. *A Two-Dimensional Model for the Combustion Chamber/Gun Tube of a Concept VIC Regenerative Liquid Propellant Gun*; BRL-TR-3341; U.S. Army Ballistic Research Laboratory: Aberdeen Proving Ground, MD, 1992.

7. Coffee, T. P. *A Combined Lumped Parameter/One-Dimensional Blowdown Model for the Regenerative Liquid Propellant Gun*; BRL-TR-3364; U.S. Army Ballistic Research Laboratory: Aberdeen Proving Ground, MD, 1992.

8. Stiefel, L. *Thermochemical and Burning Rate Properties of Deterred U.S. Small Arms Propellants*; technical report ARSCD-TR-80005; U.S. Army ARDEC: Picatinny Arsenal, NJ, 1980.

9. Oerlikon. *Oerlikon 35-mm Ammunition*. Publication WWW 400101 E 1978; Machine Tool Works Oerlikon-Buhrle Ltd.: Zurich, Switzerland, 1978.

NO. OF
COPIES ORGANIZATION

1 (PDF ONLY) DEFENSE TECHNICAL INFORMATION CTR
DTIC OCA
8725 JOHN J KINGMAN RD
STE 0944
FORT BELVOIR VA 22060-6218

1 US ARMY RSRCH DEV & ENGRG CMD
SYSTEMS OF SYSTEMS INTEGRATION
AMSRD SS T
6000 6TH ST STE 100
FORT BELVOIR VA 22060-5608

1 INST FOR ADVNCD TCHNLGY
THE UNIV OF TEXAS
AT AUSTIN
3925 W BRAKER LN
AUSTIN TX 78759-5316

1 DIRECTOR
US ARMY RESEARCH LAB
IMNE ALC IMS
2800 POWDER MILL RD
ADELPHI MD 20783-1197

3 DIRECTOR
US ARMY RESEARCH LAB
AMSRD ARL CI OK TL
2800 POWDER MILL RD
ADELPHI MD 20783-1197

ABERDEEN PROVING GROUND

1 DIR USARL
AMSRD ARL CI OK TP (BLDG 4600)

NO. OF COPIES ORGANIZATION

1 DIRECTOR
US ARMY RESEARCH LAB
AMSRD ARL D
J MILLER
2800 POWDER MILL RD
ADELPHI MD 20783-1197

3 DIRECTOR
US ARMY RESEARCH LAB
AMSRD ARL RO P
D MANN
R SHAW
TECH LIB
PO BOX 12211
RESEARCH TRIANGLE PARK NC
27709-2211

8 US ARMY AVIATN & MSLE CMD
W CHEW
C DOLBEER
J LILLY
M LYON
J FISHER
B MARSH
R MICHAELS
D THOMPSON
REDSTONE ARSENAL AL
35898-5249

2 PM MAS
SFAE AMO MAS
M BUTLER
PICATINNY ARSENAL NJ
07806-5000

2 PM CAS
SFAE AMO CAS
PICATINNY ARSENAL NJ
07806-5000

9 DIR BENET WEAPONS LAB
M AUDINO
R BERGGREN
R DILLON
R FISCELLA
R HASENBEIN
E KATHE
J MCNEIL
K MINER
S SOPOK
WATERVLIET NY
12189-4050

NO. OF COPIES ORGANIZATION

18 CDR US ARMY ARDEC
D CARLUCCI
R CARR
R CIRINCIONE
S EINSTEIN
T GORA
J HEDDERICH
P HUI
J LANNON
E LOGSDEN
P LU
B MACHAK
S NICHOLICH
P O REILLY
J O REILLY
J RUTKOWSKI
A SABASTO
J SHIN
R SURAPANENI
PICATINNY ARSENAL NJ
07806-5000

1 COMMANDER
RADFORD ARMY AMMO PLANT
SMCAR QA HI LIB
RADFORD VA 24141-0298

1 COMMANDER
US ARMY NGIC
AMXST MC 3
220 SEVENTH ST NE
CHARLOTTESVILLE VA 22901-5396

1 COMMANDANT
USAFC&S
ATSF CN
P GROSS
FT SILL OK 73503-5600

2 CDR NAVAL RSRCH LAB
TECH LIB
J BORIS
WASHINGTON DC 20375-5000

1 OFFICE OF NAVAL RSRCH
J GOLDWASSER
875 N RANDOLPH ST RM 653
ARLINGTON VA 22203-1927

NO. OF COPIES ORGANIZATION

6 CDR
NSWC
R DOHERTY
C GOTZMER
S MITCHELL
S PETERS
C WALSH
TECH LIB
INDIAN HEAD MD 20640-5000

4 CDR
NSWC
J FRAYSEE G33
R FRANCIS T08
T TSCHIRN G30
TECH LIB
DAHLGREN VA 22448-5000

3 CDR
NAVAL AIR WARFARE CTR
A ATWOOD
S BLASHILL
T PARR
CH1NA LAKE CA 93555-6001

1 AIR FORCE RSRCH LAB
MNME EN MAT BR
B WILSON
2306 PERIMETER RD
EGLIN AFB FL 32542-5910

1 AIR FORCE OFC OF SCI RSRCH
M BERMAN
875 N RANDOLPH ST
SUITE 235 RM 3112
ARLINGTON VA 22203-1768

1 NASA LANGLEY RSRCH CTR
D BUSHNELL
MS 110
HAMPTON VA 23681-2199

1 DIR SANDIA NATL LAB
M BAER
DEPT 1512
PO BOX 5800
ALBUQUERQUE NM 87185

2 DIR LAWRENCE LIVERMORE NL
L FRIED
M MURPHY
PO BOX 808
LIVERMORE CA 94550-0622

NO. OF COPIES ORGANIZATION

1 CENTRAL INTELLIGENCE AGNCY
J BACKOFEN
RM 4PO7 NHB
WASHINGTON DC 20505

1 BATTELLE EAST SCI & TECH
A ELLIS
1204 TECHNOLOGY DR
ABERDEEN MD 21001-1228

2 JHU CHEM PROP INFO AGNCY
W HUFFERD
R FRY
10630 LITTLE PATUXENT PKWY
STE 202
COLUMBIA MD 21044-3200

1 OUSD (AT&L)/STRAT & TACT
SYS MUNITIONS
T MELITA
3090 DEFENSE PENTAGON
RM 3B1060
WASHINGTON DC 20301-3090

1 BRIGHAM YOUNG UNIV
DEPT OF CHEMICAL ENGRG
M BECKSTEAD
PROVO UT 84601

1 CALIF INST OF TECH
F E C CULICK
204 KARMAN LAB
MS 301 46
1201 E CALIFORNIA ST
PASADENA CA 91109

2 UNIV OF ILLINOIS
DEPT OF MECH INDUSTRY
ENGRNG
H KRIER
R BEDDINI
144 MEB 1206 N GREEN ST
URBANA IL 61801-2978

5 PENN ST UNIV
DEPT OF MECH ENGRG
K KUO
T LITZINGER
G SETTLES
S THYNELL
V YANG
UNIV PARK PA 16802-7501

NO. OF COPIES ORGANIZATION

1 ARROW TECH ASSOC INC
1233 SHELBURNE RD D 8
S BURUNGTON VT 05403

1 ALLEGHENY BALLISTICS LAB
PO BOX 210
ROCKET CENTER WV 26726

1 ATK ORDNANCE
C CANDLAND
4700 NATHAN LN
PLYMOUTH MN 55442

3 ATK AMMO & ENERGETICS
RADFORD ARMY AMMO PLANT
D WORRELL
W WORRELL
S RITCHIE
RT 114 PO BOX 1
RADFORD VA 24141-0299

1 ATK THIOKOL
P BRAITHWAITE
R WARDLE
PO BOX 707
BRIGHAM CITY UT 84302-0707

1 ATK ELKTON
J HARTWELL
PO BOX 241
ELKTON MD 21921-0241

1 BAE ARMAMENT SYS DIV
J DYVIK
4800 E RIVER RD
MINNEAPOLIS MN 55421-1498

2 GEN DYNAMICS ORD/TACT SYS
N HYLTON
J BUZZETT
10101 DR M L KING ST N
ST PETERSBURG FL 33716

3 GENERAL DYNAMICS ST MARKS
J DRUMMOND
H RAINES
D W WORTHINGTON
PO BOX 222
SAINT MARKS FL 32355-0222

1 GENERAL DYNAMICS ARM SYS
J TALLEY
128 LAKESIDE AVE
BURLINGTON VT 05401

NO. OF COPIES ORGANIZATION

1 HICKS AND ASSOC SAIC
I MAY
7990 SCIENCE APPLIC CT
VIENNA VA 22182

1 PAUL GOUGH ASSOC INC
P GOUGH
1048 SOUTH ST
PORTSMOUTH NH 03801-5423

2 VERITAY TECH INC
R SALIZONI
J BARNES
4845 MILLERSPORT HWY
E AMHERST NY 14501-0305

1 SRI INTRNTL
PROPULSION SCIENCES DIV
TECH LIB
333 RAVENWOOD AVE
MENLO PARK CA 94025-3493

ABERDEEN PROVING GROUND

1 CDR USAATC
STECS LI
R HENDRICKSEN
APG MD 21005

44 DIR USARL
AMSRD ARL WM
W CIEPIELA
D LYON
AMSRD ARL WM B
J MORRIS
M ZOLTOSKI
AMSRD ARL WM BA
T KOGLER
AMSRD ARL WM BC
P PLOSTINS
AMSRD ARL WM BD
W ANDERSON
R BEYER
A BRANT
S BUNTE
T COFFEE (5 CPS)
J COLBURN
P CONROY
N ELDREDGE
B FORCH
B HOMAN
A HORST
S HOWARD

NO. OF
COPIES ORGANIZATION

P KASTE
A KOTLAR
C LEVERITT
R LIEB
K MCNESBY
M MCQUAID
A MIZIOLEK
J NEWBERRY
M NUSCA
R PESCE-RODRIGUEZ
G REEVES
B RICE
R SAUSA
J SCHMIDT
A WILLIAMS
AMSRD ARL WM BF
D WILKERSON
AMSRD ARL WM EG
E SCHMIDT
AMSRD ARL WM M
S MCKNIGHT
AMSRD ARL WM SG
T ROSENBERGER
AMSRD ARL WM T
B BURNS
P BAKER
A BIRK

INTENTIONALLY LEFT BLANK.